Supporting information for

Structural, thermal, dielectric and phonon properties of perovskite-like imidazolium magnesium formate

Mirosław Mączka,[a] Nathalia Leal Marinho Costa,[b] Anna Gągor,[a] Waldeci Paraguassu,[b] Adam Sieradzki,[c] and Jerzy Hanuza[d]*

[a]*Institute of Low Temperature and Structure Research, Polish Academy of Sciences, Box 1410, 50-950 Wrocław 2, Poland*

[b]*Faculdade de Física, Universidade Federal do Pará, 66075-110, Belém, PA, Brazil*

[c]*Department of Experimental Physics, Wrocław University of Technology, Wybrzeże Wyspiańskiego 27, 50-370, Wrocław, Poland*

[d]*Department of Bioorganic Chemistry, Faculty of Industry and Economics, Wrocław University of Economics, 118/120 Komandorska Str., 53-345 Wrocław, Poland*

e-mail: m.maczka@int.pan.wroc.pl

Table S1. Crystal data, data collection and refinement results for imidazolium magnesium formate.

Crystal data	
Chemical formula	$C_6H_8MgN_2O_6$
M_r	228.45
Crystal system, space group	Monoclinic, $P2_1/n$
Temperature (K)	296
a, b, c (Å)	12.1246 (4), 12.2087 (5), 12.4991 (4)
β (°)	91.394 (3)
V (Å^3)	1849.64 (12)
Z	8
Radiation type	Mo $K\alpha$
μ (mm^{-1})	0.20
Crystal size (mm)	0.15 × 0.09 × 0.08
Data collection	
Diffractometer	Xcalibur, Sapphire1, long nozzle
Absorption correction	Multi-scan *CrysAlis PRO*, Agilent Technologies, Empirical absorption correction using spherical harmonics, implemented in SCALE3 ABSPACK scaling algorithm.
T_{min}, T_{max}	0.981, 1.000
No. of measured, independent and observed [$I > 2\sigma(I)$] reflections	17019, 3500, 2290
R_{int}	0.056
$(\sin \theta/\lambda)_{max}$ (Å^{-1})	0.610
Refinement	
$R[F^2 > 2\sigma(F^2)]$, $wR(F^2)$, S	0.046, 0.114, 1.02
No. of reflections	3500
No. of parameters	271
H-atom treatment	H-atom parameters constrained
$\Delta\rho_{max}$, $\Delta\rho_{min}$ (e Å^{-3})	0.29, -0.25

Computer programs: *CrysAlis PRO*, Agilent Technologies, Version 1.171.37.35h (release 09-02-2015 CrysAlis171 .NET) (compiled Feb 9 2015, 16:26:32), *SHELXL2014*/7 (Sheldrick, 2014).

Table S2. Selected geometric parameters (Å, º)

Mg1—O2	2.0450 (19)	O9—C5^{ii}	1.226 (3)
Mg1—O12	2.0512 (19)	O10—C4^{iii}	1.231 (3)
Mg1—O6	2.0647 (19)	O11—C3^{iv}	1.216 (3)
Mg1—O4	2.0668 (19)	O12—C2^{v}	1.225 (3)
Mg1—O3	2.0743 (19)	C2—O12^{vi}	1.225 (3)
Mg1—O5	2.0836 (18)	C3—O11^{iv}	1.216 (3)
Mg2—O8	2.045 (2)	C4—O10^{iii}	1.231 (3)
Mg2—O10	2.0528 (19)	C5—O9^{vii}	1.226 (3)
Mg2—O9	2.0570 (19)	C6—O8^{viii}	1.225 (3)
Mg2—O7	2.0583 (19)	N7—C11	1.295 (4)
Mg2—O11	2.0746 (19)	N7—C8	1.338 (4)
Mg2—O1	2.0925 (19)	C8—C9	1.331 (4)
O1—C1	1.246 (3)	C9—N10	1.350 (4)
O2—C6	1.212 (3)	N10—C11	1.295 (4)
O3—C4	1.247 (3)	N12—C13	1.314 (4)
O4—C3	1.243 (3)	N12—C16	1.344 (4)
O5—C5	1.233 (3)	C13—N14	1.324 (4)
O6—C1	1.223 (3)	N14—C15	1.335 (4)
O7—C2	1.214 (3)	C15—C16	1.311 (4)
O8—C6^{i}	1.225 (3)		
O2—Mg1—O12	95.34 (8)	O11—Mg2—O1	88.89 (8)
O2—Mg1—O6	173.41 (8)	C1—O1—Mg2	131.05 (18)
O12—Mg1—O6	91.12 (8)	C6—O2—Mg1	137.79 (19)
O2—Mg1—O4	88.78 (8)	C4—O3—Mg1	137.28 (18)
O12—Mg1—O4	95.58 (8)	C3—O4—Mg1	133.90 (18)
O6—Mg1—O4	89.31 (8)	C5—O5—Mg1	142.37 (19)
O2—Mg1—O3	91.12 (8)	C1—O6—Mg1	132.97 (18)
O12—Mg1—O3	83.17 (8)	C2—O7—Mg2	145.0 (2)
O6—Mg1—O3	90.93 (8)	C6^{i}—O8—Mg2	139.4 (2)
O4—Mg1—O3	178.73 (8)	C5^{ii}—O9—Mg2	144.11 (19)
O2—Mg1—O5	83.97 (8)	C4^{iii}—O10—Mg2	133.57 (18)
O12—Mg1—O5	174.55 (8)	C3^{iv}—O11—Mg2	139.16 (19)
O6—Mg1—O5	89.72 (8)	C2^{v}—O12—Mg1	147.60 (19)
O4—Mg1—O5	89.81 (8)	O6—C1—O1	126.2 (3)
O3—Mg1—O5	91.43 (8)	O7—C2—O12^{vi}	127.6 (3)
O8—Mg2—O10	90.25 (8)	O11^{iv}—C3—O4	127.0 (3)
O8—Mg2—O9	93.65 (9)	O10^{iii}—C4—O3	125.9 (3)
O10—Mg2—O9	93.93 (8)	O9^{vii}—C5—O5	126.2 (3)
O8—Mg2—O7	90.46 (9)	O2—C6—O8^{viii}	128.8 (3)
O10—Mg2—O7	91.19 (8)	C11—N7—C8	109.7 (3)
O9—Mg2—O7	173.42 (9)	C9—C8—N7	106.9 (3)
O8—Mg2—O11	89.87 (8)	C8—C9—N10	105.9 (3)
O10—Mg2—O11	179.48 (8)	C11—N10—C9	109.7 (3)
O9—Mg2—O11	86.56 (8)	N7—C11—N10	107.7 (3)
O7—Mg2—O11	88.31 (8)	C13—N12—C16	108.8 (3)
O8—Mg2—O1	177.05 (9)	N12—C13—N14	107.3 (3)
O10—Mg2—O1	90.97 (8)	C13—N14—C15	108.5 (3)
O9—Mg2—O1	88.95 (8)	C16—C15—N14	108.0 (3)
O7—Mg2—O1	86.82 (8)	C15—C16—N12	107.4 (3)

Symmetry code(s): (i) *x*-1, *y*, *z*; (ii) *x*-1/2, -*y*+1/2, *z*-1/2; (iii) -*x*, -*y*+1, -*z*; (iv) -*x*, -*y*, -*z*; (v) *x*+1/2, -*y*+1/2, *z*-1/2; (vi) *x*-1/2, -*y*+1/2, *z*+1/2; (vii) *x*+1/2, -*y*+1/2, *z*+1/2; (viii) *x*+1, *y*, *z*.

Table S3. Selected hydrogen-bond parameters

D—H···*A*	*D*—H (Å)	H···*A* (Å)	*D*···*A* (Å)	*D*—H···*A* (°)
N7—H7···O4[i]	0.86	1.91	2.751 (3)	166.6
N10—H10···O3[ii]	0.86	2.00	2.820 (3)	158.9
C11—H11···O7	0.93	2.30	3.111 (4)	145.5
N12—H12···O5[iii]	0.86	2.02	2.873 (3)	170.6
N14—H14···O1[iv]	0.86	1.92	2.778 (3)	175.7
C16—H16···O8[v]	0.93	2.31	3.176 (4)	155.2

Symmetry code(s): (i) *x*-1, *y*, *z*; (ii) *x*-1/2, -*y*+1/2, *z*+1/2; (iii) -*x*+1, -*y*+1, -*z*; (iv) *x*+1/2, -*y*+1/2, *z*-1/2; (v) -*x*, -*y*+1, -*z*.

Table S4. IR and Raman wavenumebrs (in cm^{-1}) of ImMg and suggested assignments.[a]

Raman 490 K	Raman 300 K	IR 500 K	IR 300 K	assignment
3183w	3190w			ν(C-H)
3150m	3161m, 3151sh	3149w	3157w, 3143w	ν(C-H)
	3126w			ν(N-H)
3030vw	3032vw			overtone
2964w	2968w	2960w	2968w	ν(N-H)
2852s	2877sh, 2863s		2860w	$\nu_1(HCOO^-)$
		2838w	2830m	ν(N-H)
2829s	2829s			$\nu_1(HCOO^-)$
2710w	2719w, 2697w			$2\nu_2(HCOO^-)$
		1617vs	1613vs	$\nu_4(HCOO^-)$
1585w	1588w			ring stretch
1524vw	1527vw			ring stretch
1443m	1460sh, 1451m	1436w	1459w, 1440w	δ(N-H), ring stretch
	1440sh			
1392s	1386s, 1382sh, 1376sh	1378m	1382s	$\nu_5(HCOO^-)$
1357m	1353m	1358s	1358s	$\nu_2(HCOO^-)$
1264w	1271w			δ(C-H)

1251w	1254w			δ(C-H)
1194m	1203m, 1186sh	1192sh, 1181w	1204w, 1181w	δ(C-H), ring deformation
1118w	1129w	1115vw	1127w, 1115w	δ(C-H), ring deformation
1098w	1114w, 1093w	1096w	1092w	δ(C-H), ring deformation
1064w	1065w			$\nu_6(HCOO^-)$
1057w	1056w	1054w	1057w	ring deformation
		984sh, 953m	988m, 961sh	γ(N-H), ring deformation
910sh	910sh		911w	ring deformation
901w	901w	899vw	899w	ring deformation
	881vw, 862vw		861sh	ring deformation
		838m	845m	γ(N-H), ring deformation
796w	804w, 798w	799s	802s	$\nu_3(HCOO^-)$
		775sh	772w	ring deformation
631sh, 627w	634sh, 627w	629m	636m	ring torsion
	244w			$L(HCOO^-)$ and $T'(HCOO^-)$
203m	205m			$L(HCOO^-)$ and $T'(HCOO^-)$
157sh	168s			$L(HCOO^-)$
137s	134m			$L(HCOO^-)$
	82s			$L(HCOO^-)$

[a]Key: s, strong; m, medium; w, weak; vw, very weak; sh, shoulder; b, broad; Vibrations of the HCOO- ions are: C-H stretching (ν_1), symmetric C-O stretching (ν_2), antisymmetric C-O stretching (ν_4), symmetric O-C-O bending (ν_3), C-H in-plane bending (ν_5) and C-H out-of-plane bending (ν_6). Vibrations of imidazolium cation are classified as stretching (ν), in-plane bending (δ) and out-of-plane bending (γ) modes of the N-H and C-H groups as well as ring stretching,

Table S5. Wavenumber intercepts at zero pressure (ω_0) and pressure coefficients ($\alpha=d\omega/dP$), obtained from fitting of the experimental data by linear functions, for the ambient and high-pressure phases of ImMg.

ambient pressure phase		Intermediate phase		high-pressure phase		assignment
ω_0 (cm^{-1})	α ($cm^{-1}GPa^{-1}$)	ω_0 (cm^{-1})	α ($cm^{-1}GPa^{-1}$)	ω_0 (cm^{-1})	α ($cm^{-1}GPa^{-1}$)	
1459.6	1.85	1460.3	1.64	1464.6	2.70	δ(N-H), ring stretch
1449.6	2.51	1453.6	1.50	1457.6	2.02	δ(N-H), ring stretch
1436.6	2.22	1435.3	2.64	1449.1	0.96	δ(N-H), ring stretch
1386.6	3.47	1385.0	4.57	1389.9	3.34	$\nu_5(HCOO^-)$
1375.2	2.13	1372.5	4.02	1371.8	4.51	$\nu_5(HCOO^-)$
				1367.5	3.32	$\nu_5(HCOO^-)$
				1377.1	1.62	$\nu_5(HCOO^-)$
		1225.9	2.93			δ(C-H), ring deformation
1205.5	2.82	1201.9	4.29	1204.5	3.98	δ(C-H), ring deformation
				1196.0	2.92	δ(C-H), ring deformation
				1187.5	0.91	δ(C-H), ring deformation
				1136.2	3.55	δ(C-H), ring deformation
1132.6	2.72	1129.2	3.51			δ(C-H), ring deformation
1115.5	2.56			1099.9	3.35	δ(C-H), ring deformation
1090.0	3.18	1077.9	6.23	1097.4	1.66	δ(C-H), ring deformation
				1107.1	-1.27	δ(C-H), ring deformation
1065.7	1.29	1068.3	0.52	1072.6	-0.77	$\nu_6(HCOO^-)$
1056.0	1.10			1042.2	0.72	ring deformation
898.7	1.45	899.1	1.07	895.7	1.60	ring deformation
855.6	2.63	860.3	0.86	828.1	5.70	ring deformation
				845.4	2.15	ring deformation
804.7	0.86	806.1	0.36	788.7	2.69	$\nu_3(HCOO^-)$
				794.0	-1.14	$\nu_3(HCOO^-)$
637.6	0.88	632.6	3.43			ring torsion
625.9	2.60	628.9	2.21	625.6	2.70	ring torsion
				621.6	2.03	ring torsion
				622.9	1.01	ring torsion
				216.8	12.76	$L(HCOO^-)$ and $T'(HCOO^-)$

				277.1	4.72	L($HCOO^-$) and T'($HCOO^-$)
				240.8	6.75	L($HCOO^-$) and T'($HCOO^-$)
				226.4	6.80	L($HCOO^-$) and T'($HCOO^-$)
		198.8	11.02	199.9	7.82	L($HCOO^-$) and T'($HCOO^-$)
				201.1	5.63	L($HCOO^-$) and T'($HCOO^-$)
207.9	1.40	208.3	1.93	210.4	2.38	L($HCOO^-$) and T'($HCOO^-$)
166.3	2.93	149.8	7.07	126.7	9.46	L($HCOO^-$)
		135.6	6.57	123.9	8.38	L($HCOO^-$)
				137.0	5.16	L($HCOO^-$)
				167.6	-0.27	L($HCOO^-$)
136.5	1.21	139.1	-0.21	109.6	6.07	L($HCOO^-$)
				107.2	2.98	L($HCOO^-$)
				85.7	3.66	L($HCOO^-$)

.

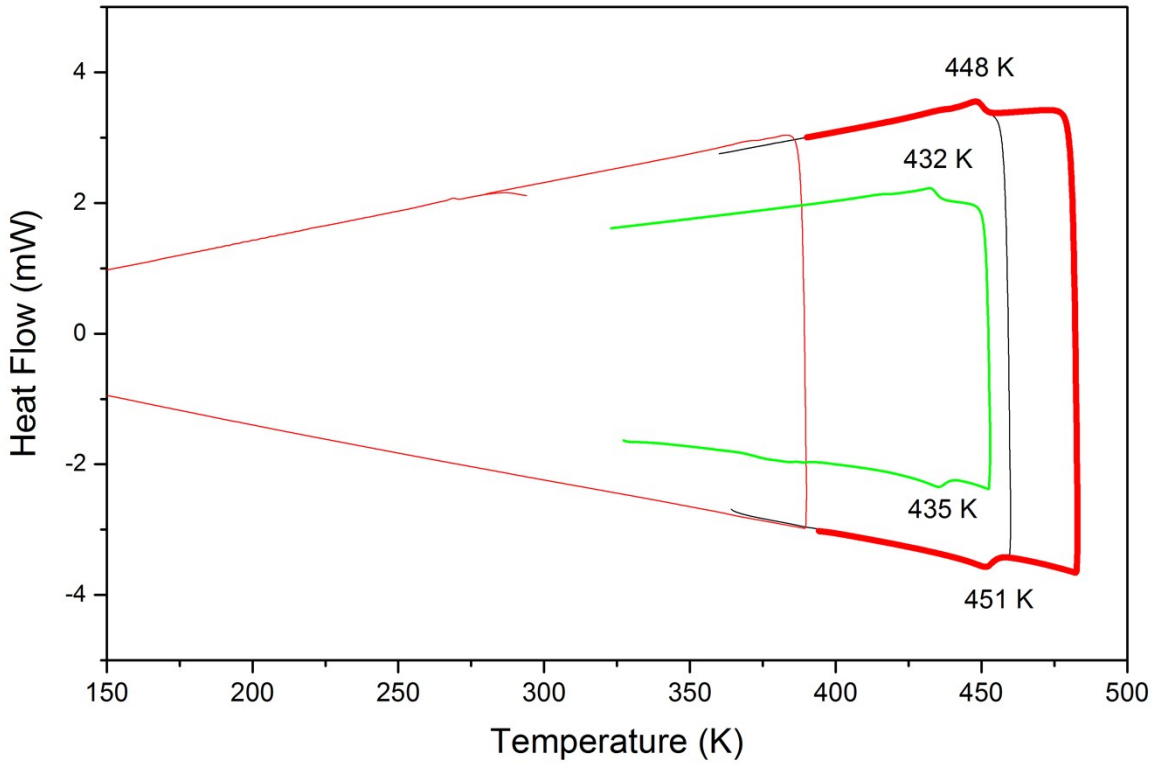

Figure S1. DSC traces for ImMg (red) and ImMn (green) in heating and cooling mode.

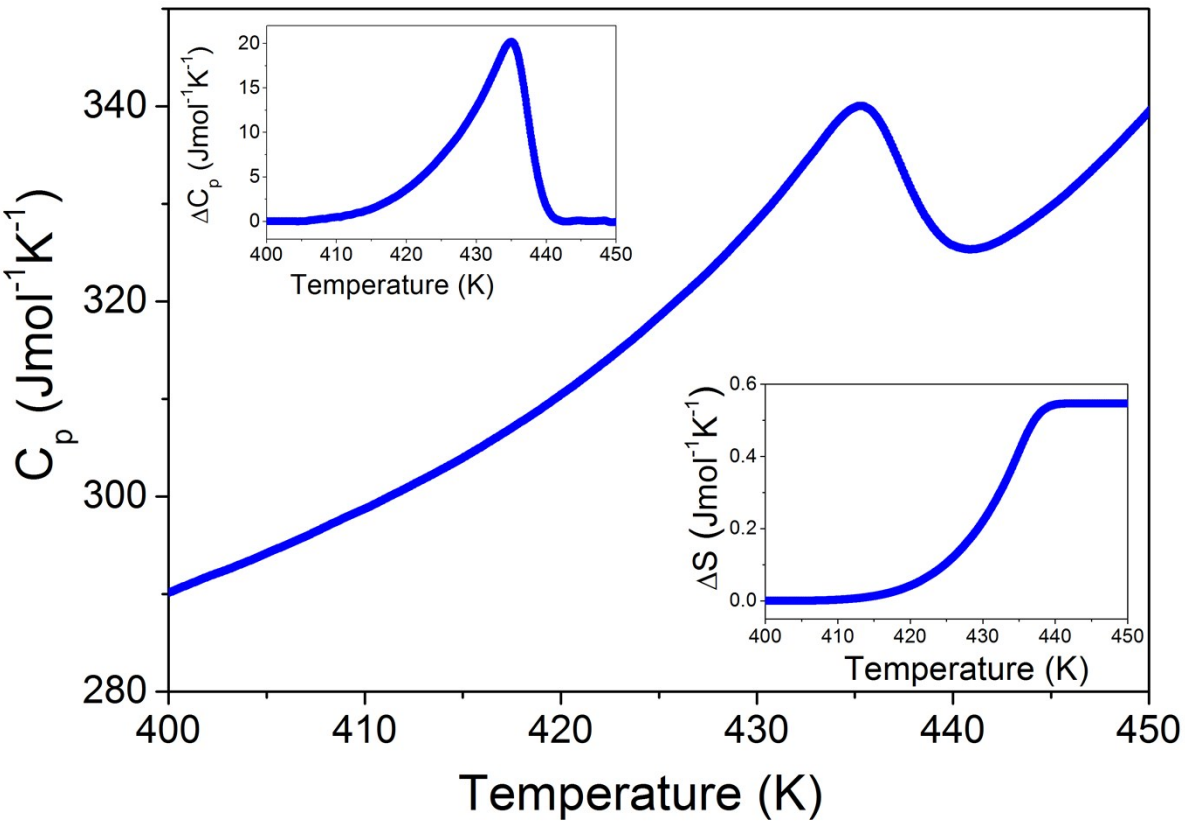

Figure S2. The heat capacity of ImMn measured in a heating mode. The estimated value of ΔH and ΔS is about ~235 Jmol^{-1} and ~0.55 Jmol^{-1}K^{-1}, respectively. Significantly smaller values of ΔH and ΔS (26.4 Jmol^{-1} and ~0.073 Jmol^{-1}K^{-1}, respectively) were reported previously (see F.-F. Wang, C. Chen, Y. Zhang, H.-Y. Ye, Q. Ye, D.-W. Fu, *J. Mater. Chem. C* 2015, **3,** 6350-6358.).

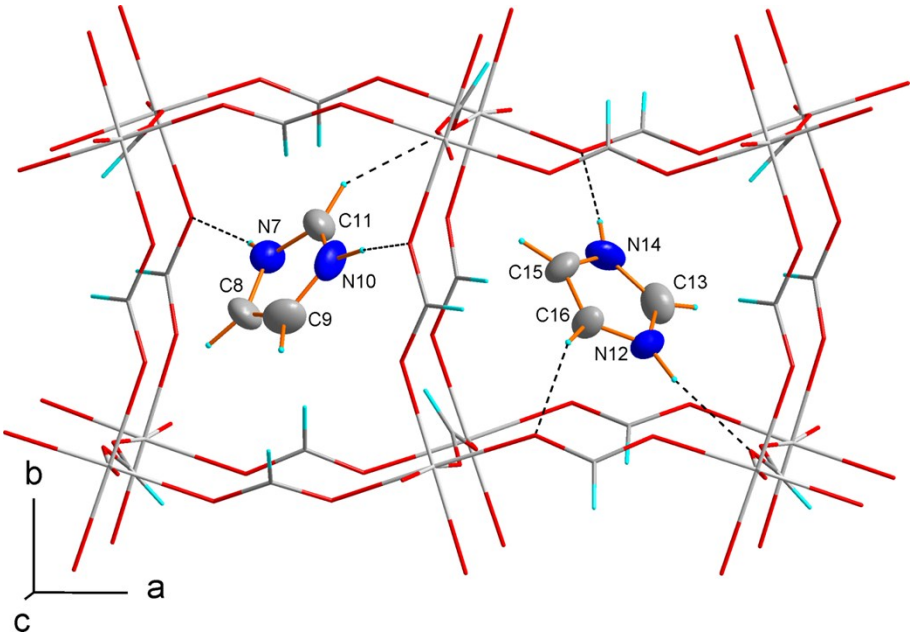

Figure S3. Two symmetry-independent imidazolium cations in the perovskite-like cavities of the $Mg(HCOO)_3^-$ framework. The dashed lines stand for the hydrogen bonds, T=296 K.

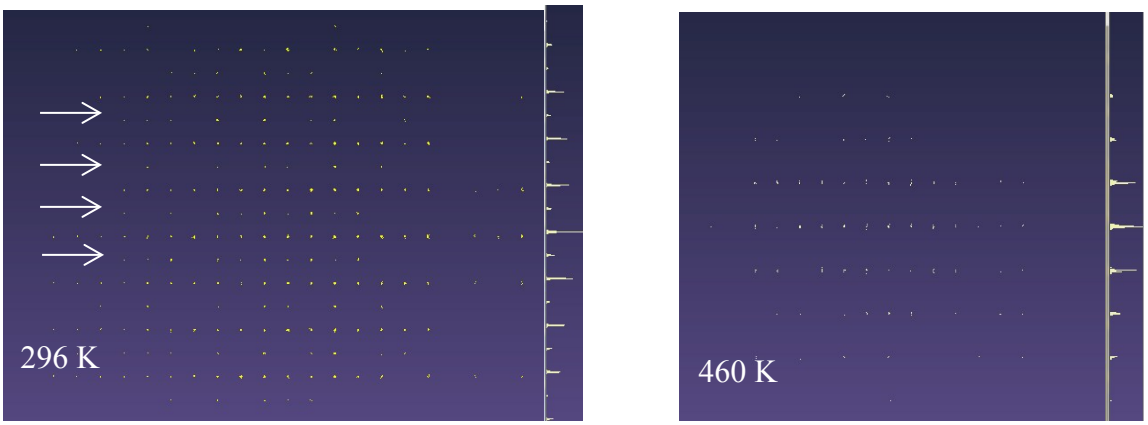

Figure S4. The reciprocal lattice of ImMg at room temperature and at 460 K. The view is along a^* axis. After the phase transition to the high-temperature phase, the hkl layers with l=2n+1 (marked by the arrows) vanish indicating that the unit cell in the *c* direction is halved.

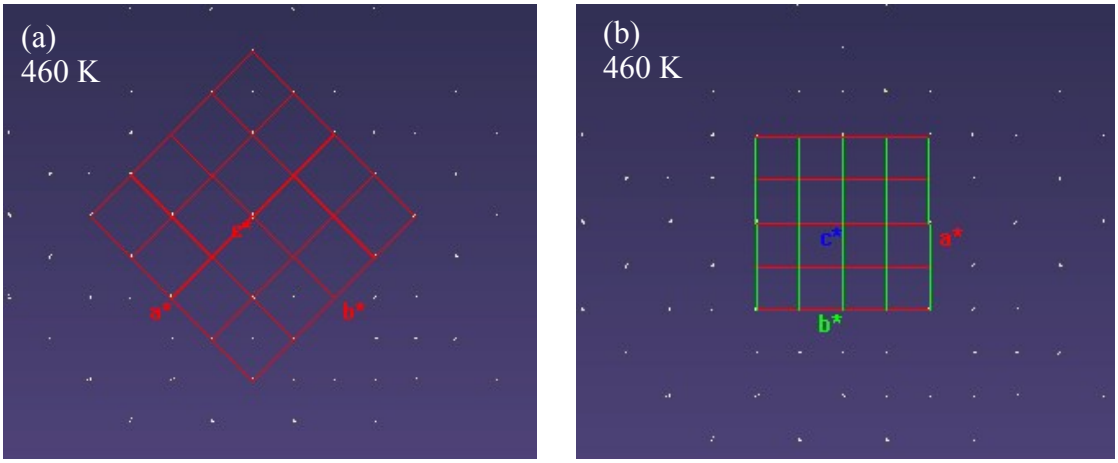

Figure S5. The reciprocal lattice of ImMg at high-temperature phase, T=460K. Two unit cell choices are presented. (a) the 'tetragonal' cell from Fang-Fang Wang et al. [33] (b) the monoclinic cell halved in the c direction with a=12.261(7) Å, b=12.290(4) Å, c=6.280(4) Å, β=90.62(5)º. The 'tetragonal 'cell skips a number of measured diffraction peaks and the lattice parameters, especially the angles, significantly depart from the tetragonal ones: a=8.683(7) Å, b=8.659(5) Å, c=6.280(4) Å, α=89.60(7) º, β=89.48(7)º, γ=90.30(6) º.

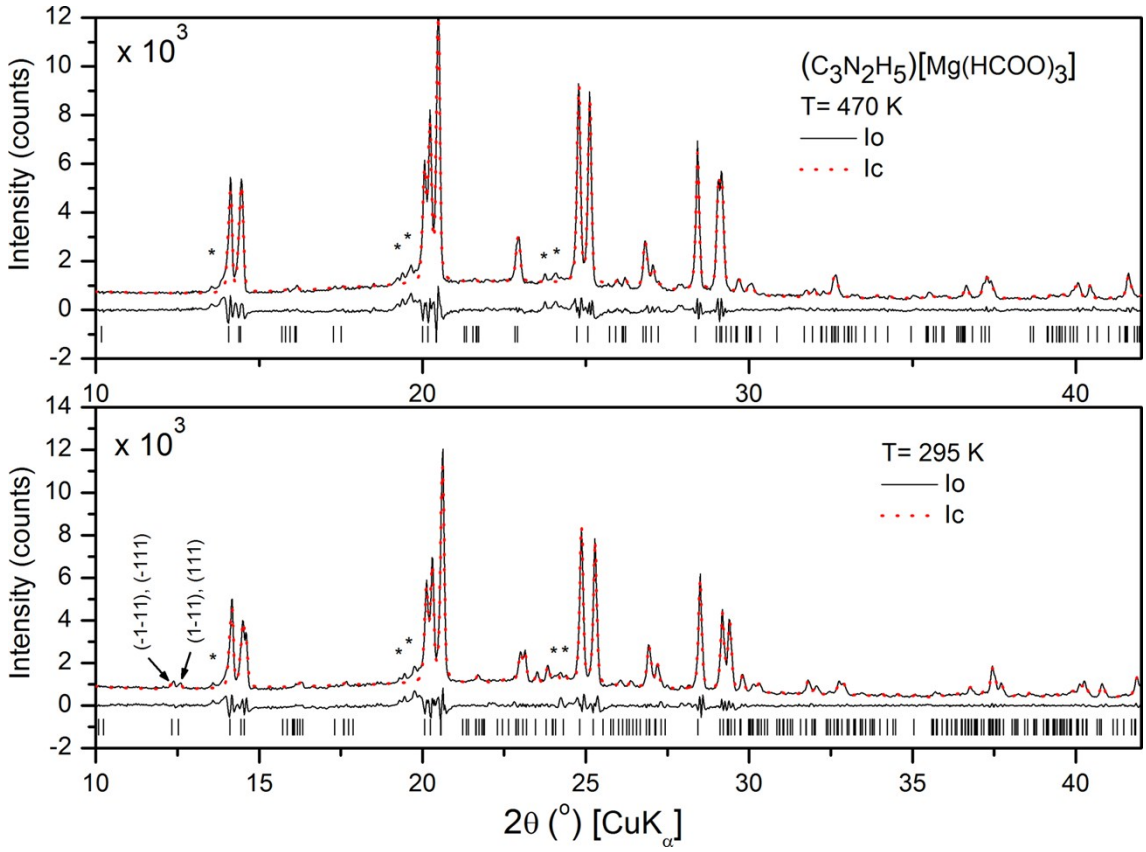

Figure S6. The results of the La Bail fit for the high (on the top) and the low-temperature phase (on the bottom) of ImMg. The obtained parameters at 470 K are: a=12.267(1) Å, b=12.308(1) Å, c=6.290(1) Å, β=91.15(1)º, V=949.6(2) Å^3, *GOF*=2.88 *Rp*=5.98 *wRp*=8.59; the parameters for the low-temperature phase are: a=12.174(1) Å, b=12.259(1) Å, c=12.549(1) Å, β=91.40(1)º, V=1872.3(3) Å^3, *GOF*=2.30, *Rp*=5.24, *wRp*=7.57. The asterisks mark the impurity phase. The most evident difference between the patterns is vanishing of the (-1-11), (-111), (1-11) and (111) diffraction peaks after the phase transition signifying the reduction of the unit cell size. The fit was done using Jana2006 [Petricek, V., Dusek, M. & Palatinus, L. (2014). Z. Kristallogr. 229(5), 345-352.]

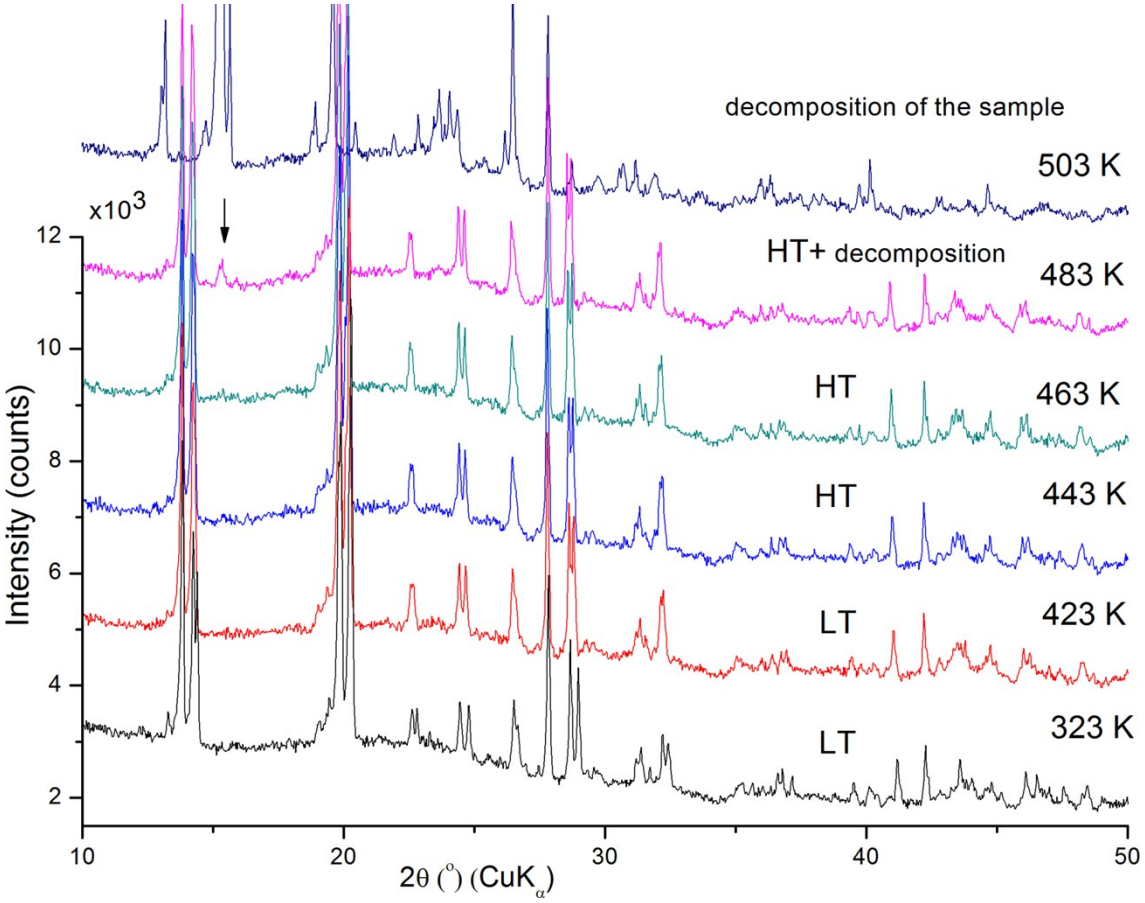

Figure S7. The x-ray diffraction patterns for ImMn. The profiles are almost identical for the high- (HT) and the low-temperature phase (LT). Any abrupt change is visible after the phase transition. The decomposition of the sample starts at 483 K; at 503 K the sample is disintegrated.

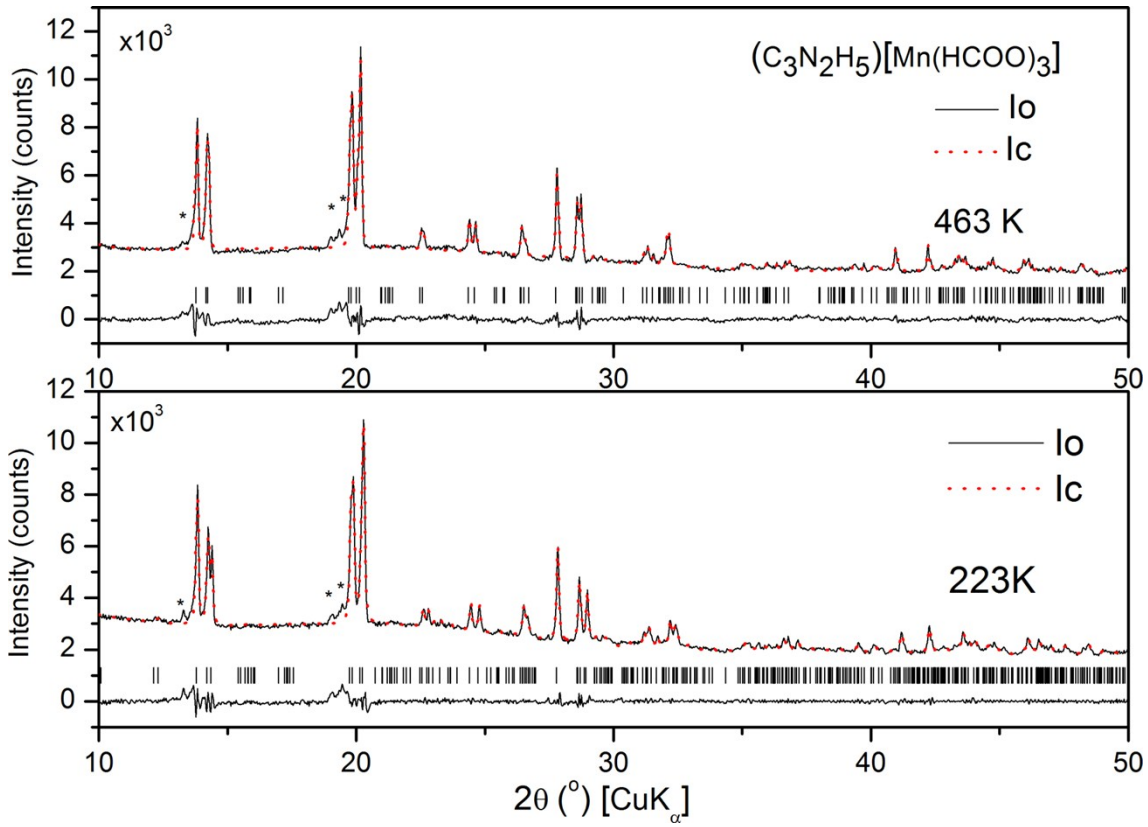

Figure S8. The results of the La Bail fit for the high (on the top) and the low-temperature phase (on the bottom) of ImMn. The obtained parameters at 463 K are: a=12.443(1) Å, b=12.505(1) Å, c=6.426(1) Å, β=90.83(1)º, V=999.7(2) Å^3, *GOF*=1.91 *Rp*=2.53 *wRp*=3.64; the parameters for the low-temperature phase are: a=12.343(1) Å, b=12.469(1) Å, c=12.842(1) Å, β=91.15(1)º, V=1975.9(3) Å^3, *GOF*=1.54, *Rp*=1.99, *wRp*=2.95. The asterisks mark the impurity phase. The fit was done using Jana2006 .

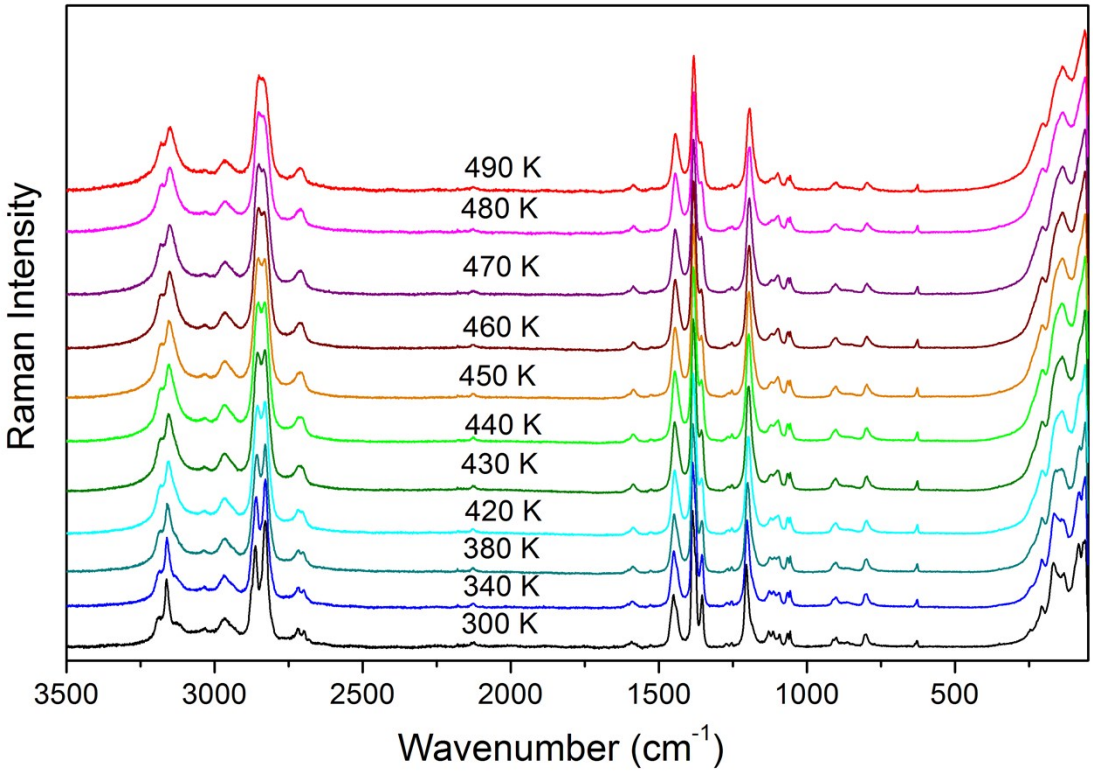

Figure S9. Raman spectra of ImMg recorded at various temperatures.

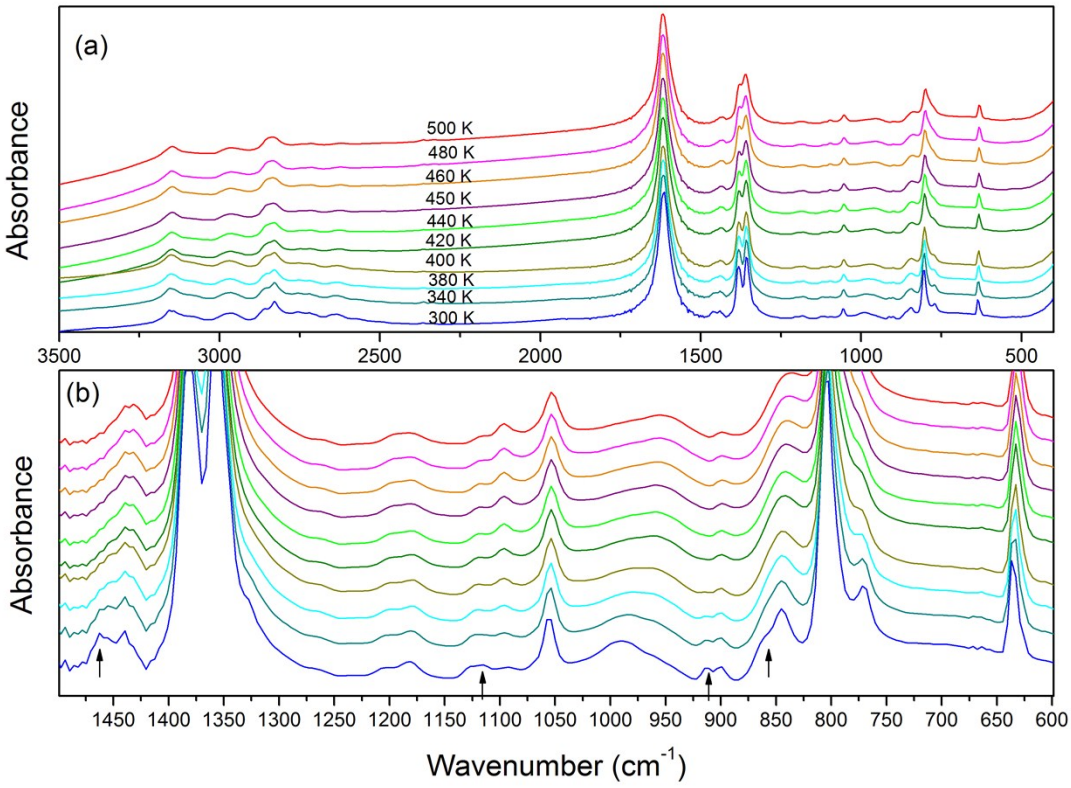

Figure S10. IR spectra of ImMg recorded at various temperatures.

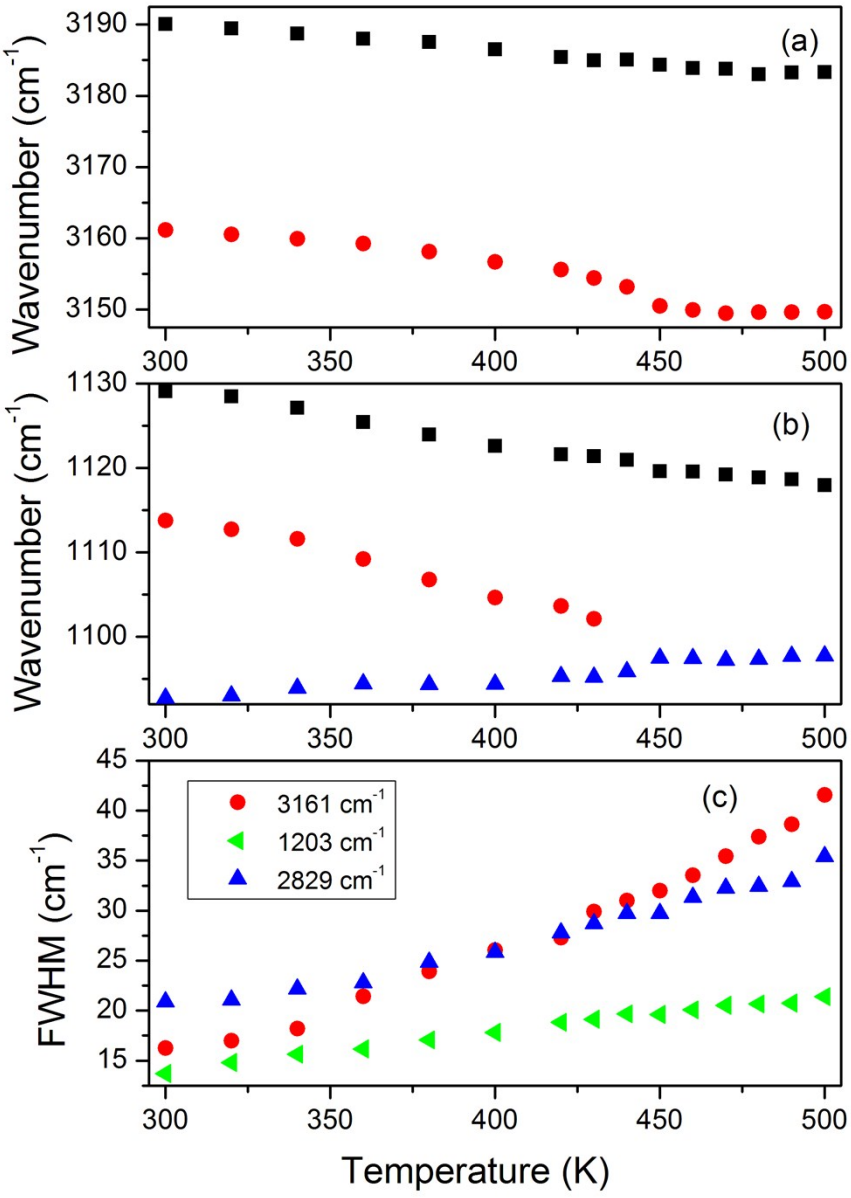

Figure S11. Temperature dependence of waveumbers for (a) the ν(C-H) and (b) δ(C-H)+ring deformation modes of imidazolium cation as well as (c) temperature dependence of FWHM values for 1203 cm^{-1} (imidazolium, δ(C-H)+ ring deformation), 2829 cm^{-1} (formate, C-H stretching vibration v_1) and 3161 cm^{-1} (imidazolium, ν(C-H)) modes.

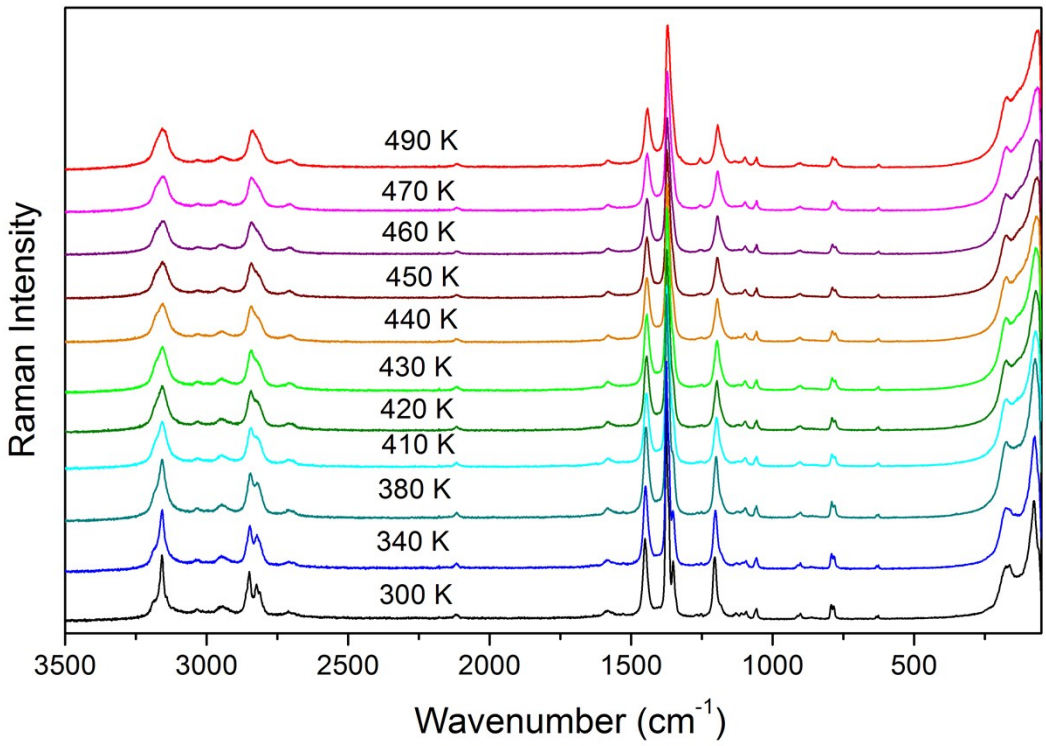

Figure S12. Raman spectra of ImMn recorded at various temperatures.

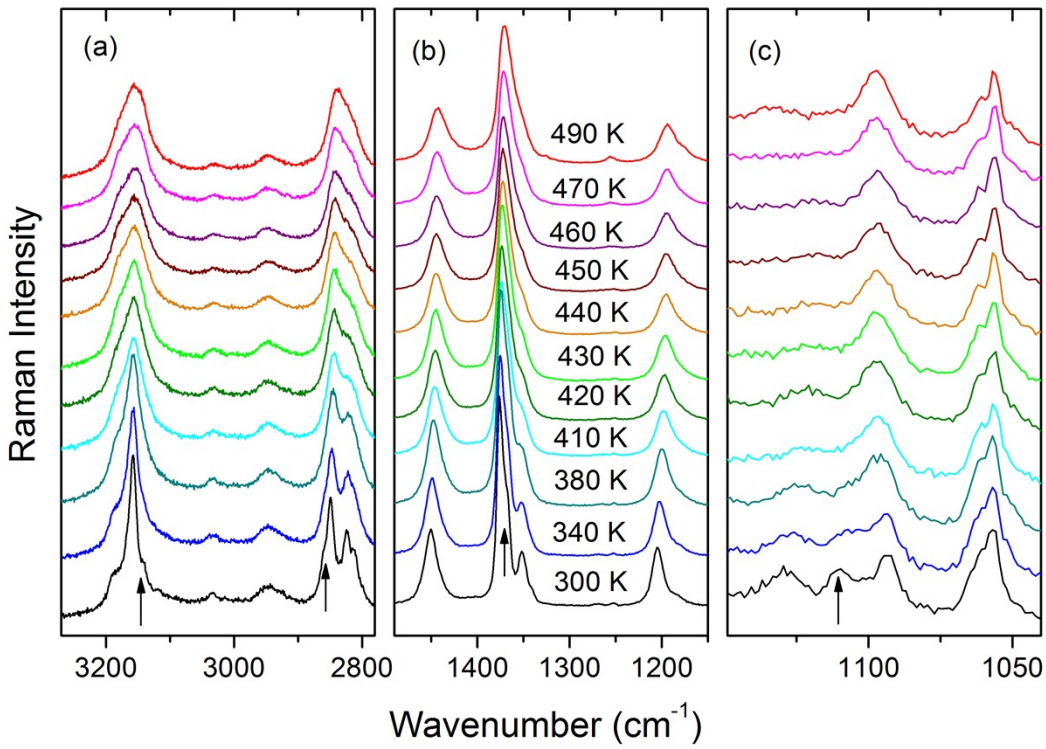

Figure S13. Detail of the Raman spectra of ImMn corresponding to the spectral ranges 2780-3270, 1150-1490 and 1040-1150 cm^{-1} at different temperatures in heating run. Arrows indicate bands that disappear as a result of the phase transition.

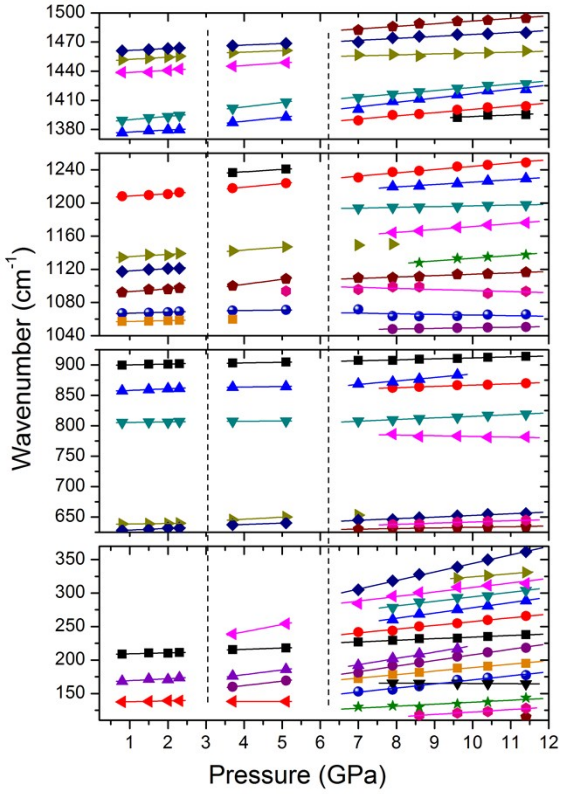

Figure S14. Wavenumber vs. pressure plots of the Raman modes observed in ImMg crystal for compression experiment. The solid lines are linear fits of the data to $\omega(P) = \omega_0+\alpha P$. Vertical lines show the pressures at which structural phase transitions occur.

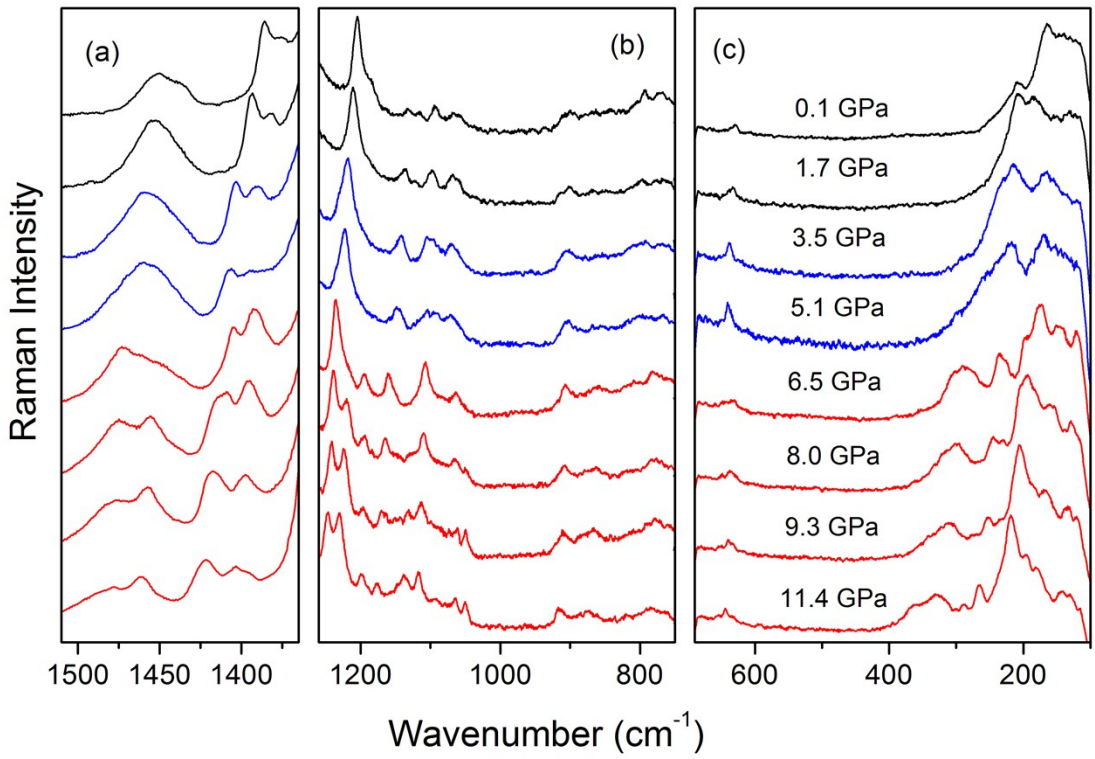

Figure S15. Raman spectra of ImMg recorded during decompression experiment.